Distributed Optimal Power Flow in Hybrid AC–DC Grids

Nico Meyer-Huebner, *Student Member, IEEE*, Michael Suriyah, *Member, IEEE*, and Thomas Leibfried, *Member, IEEE*

***Abstract*—Distributed or multi-area optimal power flow (OPF) in alternating current (AC) grids is currently a subject undergoing intense study to cope with computational burdens in large-scale grids and to maintain self-control of a regional system operator. However, future power grids will most likely be hybrid grids consisting of the conventional AC transmission system combined with high voltage direct current (DC) technology. Thus, we reformulate the full AC–DC OPF problem such that it becomes separable and, therefore, accessible to distributed algorithms. Then, we show in detail two different approaches on the decomposition of a hybrid AC–DC grid. Finally, we implement an improved alternating direction of multipliers method (ADMM) as well as the most recently proposed augmented Lagrangian based alternating direction inexact Newton (ALADIN) method. Simulation results show that optimality gaps below 0.01% are reached with both decomposition approaches and algorithms for two different test systems (5-bus and 66-bus). Furthermore, convergence rates and wall clock times are reduced by around one order of magnitude from ADMM to ALADIN.**

***Index Terms*—Distributed optimal power flow, multi-area optimal power flow, AC-DC grid, ADMM, ALADIN.**

I. Introduction

THE increasing penetration of Renewable Energy Sources leads to a transformation of the current power system. The installation of e.g. large offshore wind parks will require additional transmission capacity to supply distant load centers. In Germany, high voltage direct current (HVDC) technology will be one key to secure power supply. The resulting hybrid AC-DC grid brings up a lot of novel challenges, but also large potential in power system planning, operation and optimization.

Optimal power flow (OPF) is a powerful tool to ensure economic system operation while respecting important physical network constraints. It was introduced by Carpentier [1] and the conventional AC OPF was studied to large extents in the last decades, a review can be found in [2], [3]. Lately, the OPF problem was extended to the above stated AC-DC grid in [4]–[10] by using voltage source converters (VSCs) to transfer power between AC and DC grid. The highly controllable VSCs are used to minimize steady-state losses in [4]–[6]. In [7], the DC grid is enabled to participate in unpredictable power flow changes between scheduled power set points. AC-DC OPF is used in [8] to evaluate economic aspects when installing VSC-based DC systems in an existing AC system and the authors in [9] include energy storage systems in the hybrid grid. N-1-secure dispatch strategies for embedded DC links are presented in [10].

Due to the increasing complexity of the power system and an operation closer to network limitations, central coordination in large scale networks comes with major computational burdens. Also, privacy, e.g. for each transmission system operator (TSO) controlling a certain region, is a concern. The above reasons led to an increasing interest in distributed optimization. An early overview on distributed OPF algorithms can be found in [11] and the most recent developments are examined in detail in [12]. The most popular branches to tackle the non-convex AC OPF problem are the Optimality Condition Decomposition (OCD) [13]–[15], Auxiliary Problem Principle (APP) [16], [17] and the Alternating Direction of Multipliers Method (ADMM) [18]–[20]. In OCD technique, primal and dual variables are assigned to a specific sub-problem. During an interior point iteration, all foreign variables are fixed to their previous value. By penalizing the coupling variables in the objective, convergence is achieved under certain assumptions (e.g. relatively weakly coupled sub-problems). Those assumptions can not be guaranteed for any problem, however, the method is shown to work for certain networks up to a few hundred buses [15]. In a different way from OCD, in APP and ADMM each sub-problem uses variable duplicates from neighboring sub-problems and is solved to optimality. They are based on Augmented Lagrangian Relaxation, where penalty terms, calculated from the coupling variable deviation and their Lagrangian multipliers, are added to the objective function. The improvement from APP to ADMM is a sequential update on internal and external variables, which reduces necessary information exchange and leads to communication between neighboring regions only. Convergence is achieved in a large-scale network [20], but again, convergence guarantees can not be given for non-convex problems.

Most recently, a further development of ADMM was presented in [21], which is called Augmented Lagrangian based Alternating Direction Inexact Newton (ALADIN) method. The agents solve similar local problems compared to ADMM, but it includes elements from the field of sequential quadratic programming to improve the (central) update step. Convergence rate is much faster than in ADMM and it can be extended using

Manuscript received June 7, 2018; revised August 14, 2018, November 2, 2018, and December 13, 2018; accepted December 23, 2018. Date of publication February 11, 2019; date of current version June 18, 2019. This work was supported by the German Research Foundation (DFG) under Grant LE1432/14-2. Paper no. TPWRS-00877-2018. *(Corresponding author: Nico Meyer-Huebner.)*

The authors are with the Institute of Electric Energy Systems and High-Voltage Technology, Karlsruhe Institute of Technology, Karlsruhe 76131, Germany (e-mail: nico.meyer-huebner@kit.edu; michael.suriyah@kit.edu; thomas.leibfried@kit.edu).

Digital Object Identifier 10.1109/TPWRS.2019.2892240

globalization strategies that guarantee convergence. ALADIN was applied to the conventional OPF problem in [22], [23] and showed impressive improvement in terms of convergence speed and optimality gap. However, the communication is increased and as of now, the centralized update can not yet be entirely distributed.

In [24], an AC-DC OPF is calculated in a distributed manner. However, the AC system is approximated with a linear DC approach, which is much easier in terms of local optimization as well as network decomposition and consensus between areas. Additionally, converter losses are neglected, which further simplifies the decoupling between AC and DC regions.

Thus, the main contributions of the paper are the following:

- Reformulate the full AC-DC OPF problem such that it becomes separable
- Present detailed modeling approaches on how to partition and decouple a hybrid AC-DC grid
- Implement novel penalty scaling to improve ADMM convergence.

The rest of the paper is organized as follows. In Section II, the central AC-DC OPF problem is stated allowing for a regional formulation. In Section III, two approaches to partition AC-DC networks are presented and consensus constraints are explained. In Section IV, ADMM and ALADIN algorithms are briefly explained and in Section V, results are shown for two different test systems. Lastly, some conclusions are drawn in Section VI.

II. AC-DC Optimal Power Flow

Consider an electrical network with a total of N nodes, which are collected in the set $\mathcal{N} = \{1, ..., N\}$. We distinguish two types of nodes: alternating current (AC) nodes and direct current (DC) nodes. The subsets $\mathcal{N}^{\text{AC}} \subseteq \mathcal{N}$ and $\mathcal{N}^{\text{DC}} \subseteq \mathcal{N}$ identify the membership of a node in $\mathcal{N}$. A node can only be of one type, thus $\mathcal{N}^{\text{AC}} \cup \mathcal{N}^{\text{DC}} = \mathcal{N}$ and $\mathcal{N}^{\text{AC}} \cap \mathcal{N}^{\text{DC}} = \emptyset$. Electrical neighbors of an AC node $i \in \mathcal{N}^{\text{AC}}$ (excluding node i itself) are collected in $\mathcal{N}^{\text{AC}}(i)$. Analogously, $\mathcal{N}^{\text{DC}}(i)$ collects all DC neighbors of $i \in \mathcal{N}^{\text{DC}}$.

A. Optimization Variables

Each optimization variable can be assigned to a specific node. The variables assigned to an AC node i are

$$s_{\text{AC},i} = \{(V_{\text{AC},i}, P_{\text{G},j}, Q_{\text{G},j}, P_{\text{VSC},k}, Q_{\text{VSC},k}), \forall j \in \mathcal{E}_i^{\text{G}}, \forall k \in \mathcal{E}_i^{\text{VSC}}\}. \quad (1)$$

Here, $V_{\text{AC},i}$ is the complex voltage at node i and a generator is modeled with an active and a reactive power source $(P_{\text{G}}, Q_{\text{G}})$. Active and reactive power output of an AC-DC converter is denoted with $(P_{\text{VSC}}, Q_{\text{VSC}})$. Furthermore, $\mathcal{E}_i^{\text{type}} \subseteq \mathcal{E}^{\text{type}}$ denotes the subset of a certain type of injection variables, which is connected to node i. Note that in the centralized formulation, a converter is connected to both an AC and a DC node, thus it can be an element of both $\mathcal{E}_i^{\text{VSC}}$ and $\mathcal{E}_j^{\text{VSC}}$, where $i \in \mathcal{N}^{\text{AC}}$ and $j \in \mathcal{N}^{\text{DC}}$. The variables assigned to a DC node i are

$$s_{\text{DC},i} = \{(V_{\text{DC},i}, P_{\text{G},j}), \forall j \in \mathcal{E}_i^{\text{G}}\}, \quad (2)$$

where $V_{\text{DC},i}$ is the real voltage at node i. Note that usually we do not connect generators to a DC node. However, the supported possibility will prove useful for later purposes in distributed optimization. We generalize the node states to

$$s_i = \begin{cases} s_{\text{AC},i} & \text{if } i \in \mathcal{N}^{\text{AC}} \\ s_{\text{DC},i} & \text{if } i \in \mathcal{N}^{\text{DC}}. \end{cases} \quad (3)$$

Finally, the optimization variables in a network with node set $\mathcal{N}$ are given by

$$x_{\mathcal{N}} = \{s_i, \forall i \in \mathcal{N}\}. \quad (4)$$

B. Objective

The objective usually consists of generator fuel cost functions. However, we allow for a small weight to reactive power injections in order to regularize the problem and thus improve its numerical condition. Technically, this is motivated by keeping reactive power injections small. The local cost function at node i is

$$f_i(s_i) = \sum_{j \in \mathcal{E}_i^{\text{G}}} \left(a_{\text{G},j}(P_{\text{G},j})^2 + b_{\text{G},j} P_{\text{G},j}\right) + a_{\text{Q}} \sum_{j \in \mathcal{E}_i^{\text{G}}} (Q_{\text{G},i})^2 + a_{\text{Q}} \sum_{j \in \mathcal{E}_i^{\text{VSC}}} (Q_{\text{VSC},i})^2, \quad (5)$$

where $(a_{\text{G},j}, b_{\text{G},j})$ are cost function coefficients of a generator j and a_{Q} is the quadratic coefficient for all reactive injections. The total costs in a network with node set $\mathcal{N}$ is formed to

$$f_{\mathcal{N}}(x_{\mathcal{N}}) = \sum_{i \in \mathcal{N}^{\text{AC}}} f_i(s_i). \quad (6)$$

C. Constraints

The full constraint region for a network with node set $\mathcal{N}$ is

$$\mathcal{H}_{\mathcal{N}} = \Big\{ x_{\mathcal{N}} \quad | \quad \text{Re}\big(V_{\text{AC},i} \sum_{j \in \mathcal{N}^{\text{AC}}} (Y_{\text{AC},ij} V_{\text{AC},j})^*\big) = P_{\text{AC},i}, \quad (7a)$$

$$\text{Im}\big(V_{\text{AC},i} \sum_{j \in \mathcal{N}^{\text{AC}}} (Y_{\text{AC},ij} V_{\text{AC},j})^*\big) = Q_{\text{AC},i}, \quad (7b)$$

$$\underline{V}_{\text{AC},i} \leq |V_{\text{AC},i}| \leq \overline{V}_{\text{AC},i}, \quad (7c)$$

$$V_{\text{AC},l} = 1.0\angle 0, \quad \forall l \in \mathcal{N}^{\text{refAC}}, \quad (7d)$$

$$V_{\text{DC},j} \sum_{l \in \mathcal{N}^{\text{DC}}} (Y_{\text{DC},jl} V_{\text{DC},l}) = P_{\text{DC},j}, \quad (7e)$$

$$\underline{V}_{\text{DC},j} \leq V_{\text{DC},j} \leq \overline{V}_{\text{DC},j}, \quad (7f)$$

$$V_{\text{DC},l} = 1.0, \quad \forall l \in \mathcal{N}^{\text{refDC}}, \quad (7g)$$

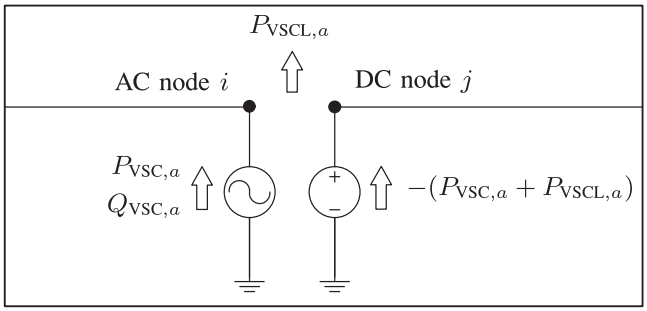

Fig. 1. Model of a converter a connecting AC node i with DC node j.

$$\underline{P}_{\text{G},l} \le P_{\text{G},l} \le \overline{P}_{\text{G},l}, \quad \forall l \in \mathcal{E}_i^{\text{G}}, \tag{7h}$$

$$\underline{Q}_{\text{G},l} \le Q_{\text{G},l} \le \overline{Q}_{\text{G},l}, \quad \forall l \in \mathcal{E}_i^{\text{G}}, \tag{7i}$$

$$\left.\begin{aligned} &P_{\text{VSC},l} + Q_{\text{VSC},l} \le \overline{S}^2_{\text{VSC},l}, \quad \forall l \in \mathcal{E}_i^{\text{VSC}}, \\ &\forall i \in \mathcal{N}^{\text{AC}}, \forall j \in \mathcal{N}^{\text{DC}} \end{aligned}\right\}. \tag{7j}$$

The power balance of active and reactive power for an AC node i is given by (7a) and (7b), respectively, where $Y_{\text{AC},ij}$ is the ij-th entry of the complex AC bus admittance matrix. Furthermore, $(P_{\text{AC},i}, Q_{\text{AC},i})$ are active and reactive power injected at node i, respectively, which are summed up to

$$P_{\text{AC},i} = \sum_{l \in \mathcal{E}_i^{\text{G}}} P_{\text{G},l} + \sum_{l \in \mathcal{E}_l^{\text{VSC}}} P_{\text{VSC},l} - \sum_{l \in \mathcal{E}_i^{\text{D}}} P_{\text{D},l} \tag{8a}$$

$$Q_{\text{AC},i} = \sum_{l \in \mathcal{E}_i^{\text{G}}} Q_{\text{G},l} + \sum_{l \in \mathcal{E}_i^{\text{VSC}}} Q_{\text{VSC},l} - \sum_{l \in \mathcal{E}_i^{\text{D}}} Q_{\text{D},l}, \tag{8b}$$

with $(P_{\text{D},l}, Q_{\text{D},l})$ the active and reactive power demand of a load l. Voltage magnitudes are limited by (7c) and both magnitude and angle are fixed for one node per synchronous area (7d). Reference nodes are collected in $\mathcal{N}^{\text{refAC}} \subset \mathcal{N}^{\text{AC}}$ and $\mathcal{N}^{\text{refDC}} \subset \mathcal{N}^{\text{DC}}$, respectively. Equivalently to the AC side, the active power balance of a DC node j is given by (7e) and $Y_{\text{DC},jl}$ is the jl-th entry of the real DC bus admittance matrix. Again, voltages are limited by (7f) and the voltage magnitude of one node is fixed to 1 pu (7g). Generator power outputs must satisfy operational upper and lower limits (7h)-(7i). The converter model is a simplified VSC model based on two generators, see Fig. 1, where a positive value of P_{VSC} denotes a power flow from DC to AC. The transferred power is reduced by a quadratic loss term P_{VSCL}, where α_{VSCL} and γ_{VSCL} are converter specific loss parameters. Thus, the injected power at DC node j becomes

$$P_{\text{DC},j} = \sum_{l \in \mathcal{E}_j^{\text{G}}} P_{\text{G},l} - \sum_{l \in \mathcal{E}_j^{\text{VSC}}} (P_{\text{VSC},l} + P_{\text{VSCL},l}). \tag{9}$$

Furthermore, we limit the apparent power injection on the AC side to $\overline{S}_{\text{VSC}}$ by (7j).

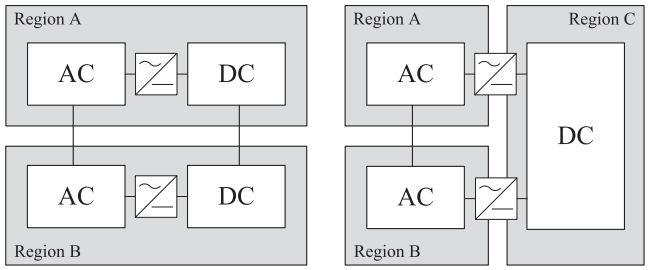

Fig. 2. Left: *Shared-DC* approach, where hybrid AC-DC regions are formed. Right: *Joint-DC* approach, where regions only contain either AC or DC nodes.

D. Problem Formulation

For later access to dual variables, we choose $h_{\mathcal{N}}(x_{\mathcal{N}})$ such that $\{x_{\mathcal{N}} | h_{\mathcal{N}}(x_{\mathcal{N}}) \le 0\} = \mathcal{H}_{\mathcal{N}}$ and obtain our problem formulation for a network with node set $\mathcal{N}$:

$$\underset{x_{\mathcal{N}}}{\text{minimize}} \quad F_{\mathcal{N}}(x_{\mathcal{N}}) \tag{10a}$$

$$\text{subject to} \quad h_{\mathcal{N}}(x_{\mathcal{N}}) \le 0. \tag{10b}$$

Note that this general formulation could just as well describe pure AC or DC networks if $\mathcal{N} = \mathcal{N}^{\text{AC}}$ or $\mathcal{N} = \mathcal{N}^{\text{DC}}$, which is important for the distributed approach.

III. Regional OPF Formulation

Finally, we form a regional formulation for the AC-DC OPF. We define R regions in $\mathcal{R} = \{1, ..., R\}$, and let $\mathcal{N}_k$ identify all nodes in region k. Herewith, $\mathcal{N}_k^{\text{AC}}$ collects all AC nodes and $\mathcal{N}_k^{\text{DC}}$ all DC nodes in region k. In the following, we first address the grid partitioning approaches and then the decoupled inter-connector models for AC-DC grids.

A. Partitioning of the Grid

We assume the number of AC regions to be inherently given by the number of TSOs or control areas. In the case of a DC grid however, we must consider different possibilities which will be subject to political will.

1) Joint-DC (J-DC): We define R^{AC} regions containing only AC nodes and R^{DC} regions containing only DC nodes, thus a total of $R = R^{\text{AC}} + R^{\text{DC}}$ regions. This approach follows the idea that there exist one or multiple independent entities which coordinate a pure DC network, see Fig. 2 (right).

2) Shared-DC (S-DC): We define $R = R^{\text{AC}}$ hybrid AC-DC regions, where each AC region may also contain DC nodes. Here, each existing TSO gains control over converters in its own control area, see Fig. 2 (left).

B. Decoupling of Inter-Regional Connectors

The decoupling between two neighboring regions *A* and *B* depends on the element which serves as inter-connector. In general, we distinguish between tie lines and converters. Let nodes $i \in \mathcal{N}_A$ and $j \in \mathcal{N}_B$ be neighbors and connect the two regions A and B.

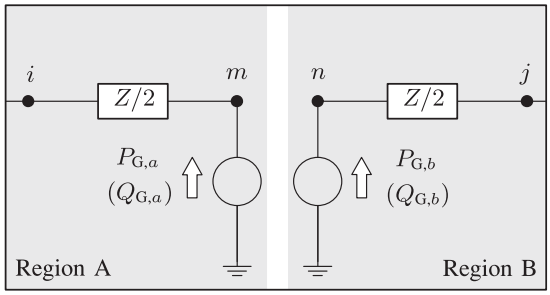

Fig. 3. Decoupling model of a tie line (AC or DC) between nodes i and j with two auxiliary nodes and two auxiliary generators.

1) AC or DC Tie Line: In [16] the decomposition method for an AC tie line using dummy generators was described. However, in [18] only voltages were used for consensus. It is not clear why the generators were omitted, but convergence rates were rather poor and the author then improved the decomposition method by including neighboring nodes from foreign regions, resulting in overlapping areas [19]. The weighted summation and difference of those two node voltages were then used for consensus and convergence could be improved. This was also adapted in [20]. However, possibly sensitive information of a neighboring region must be shared (connected loads, generators, cost functions). We therefore choose the dummy generator method for both AC and DC tie lines, see Fig. 3.

We cut the original line into two halves and add auxiliary nodes (m, n) and auxiliary generators (a, b) at both open ends. Thus, node sets are augmented to $\mathcal{N}_A \leftarrow \{\mathcal{N}_A, m\}$, $\mathcal{N}_B \leftarrow \{\mathcal{N}_B, n\}$ and the generator set is augmented to $\mathcal{E}^{\mathrm{G}} \leftarrow \{\mathcal{E}^{\mathrm{G}}, a, b\}$. To guarantee a feasible power flow, voltage must be equal at nodes m and n. Furthermore, the generators must produce the same amount of power of opposite sign. In case of an AC tie line ($i \in \mathcal{N}_A^{\mathrm{AC}}, j \in \mathcal{N}_B^{\mathrm{AC}}$), we have complex voltage and both active and reactive power for boundary conditions:

$$V_{\mathrm{AC},m} = V_{\mathrm{AC},n} \tag{11a}$$

$$P_{\mathrm{G},a} = -P_{\mathrm{G},b} \tag{11b}$$

$$Q_{\mathrm{G},a} = -Q_{\mathrm{G},b}. \tag{11c}$$

In the case of a DC tie line ($i \in \mathcal{N}_A^{\mathrm{DC}}, j \in \mathcal{N}_B^{\mathrm{DC}}$), we only have real voltage and active power to meet the constraints:

$$V_{\mathrm{DC},m} = V_{\mathrm{DC},n} \tag{12a}$$

$$P_{\mathrm{G},a} = -P_{\mathrm{G},b}. \tag{12b}$$

2) AC-DC Converter: Let VSC a connect $i \in \mathcal{N}_A^{\mathrm{AC}}$ with $j \in \mathcal{N}_B^{\mathrm{DC}}$, which separates region A from B. Then we have $a \in \mathcal{E}_i^{\mathrm{VSC}}, \mathcal{E}_j^{\mathrm{VSC}}$. We create a copy of the AC power source and add it to the DC side. This leads to a new mapping, since auxiliary VSC b is connected to the DC side instead of VSC a, which remains on the AC side. Thus, we have an augmented VSC set $\mathcal{E}^{\mathrm{VSC}} \leftarrow \{\mathcal{E}^{\mathrm{VSC}}, b\}$, leading to $a \in \mathcal{E}_i^{\mathrm{VSC}}$ and $b \in \mathcal{E}_j^{\mathrm{VSC}}$. Since the power sources point in the same direction, i.e. the AC grid,

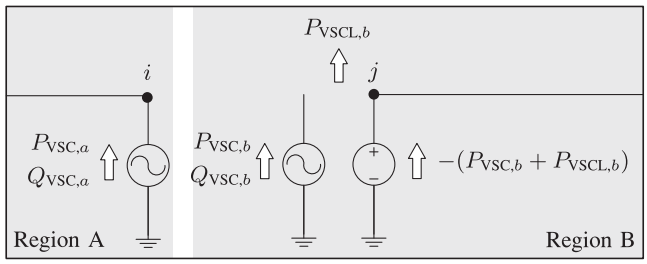

Fig. 4. Decoupled converter model following the approach *Joint DC*.

power variables on both sides must be equal:

$$P_{\mathrm{VSC},a} = P_{\mathrm{VSC},b} \tag{13a}$$

$$Q_{\mathrm{VSC},a} = Q_{\mathrm{VSC},b}. \tag{13b}$$

In a more compact form, the boundary conditions between region *A* and *B*, i.e. (11)–(13), can be written as

$$\begin{bmatrix} A_A & A_B \end{bmatrix} \begin{bmatrix} x_{\mathcal{N}_A} \\ x_{\mathcal{N}_B} \end{bmatrix} = 0. \tag{14}$$

C. Problem Formulation

Each region $k \in \mathcal{R}$ now has an extended node set $\mathcal{N}_k$, which includes all additional nodes stemming from decoupled interconnectors. For better readability, we re-define local variables, cost function and constraints of region k to

$$x_k := x_{\mathcal{N}_k} \tag{15a}$$

$$f_k(x_k) := f_{\mathcal{N}_k}(x_{\mathcal{N}_k}) \tag{15b}$$

$$h_k(x_k) := h_{\mathcal{N}_k}(x_{\mathcal{N}_k}). \tag{15c}$$

Equation (14) can be generalized for region set $\mathcal{R}$ to

$$\sum_{k \in \mathcal{R}} A_k x_k = 0. \tag{16}$$

Finally, we combine the local (independent) OPF constraints $h_k(x_k) \leq 0$ with the global consensus constraints (16) and obtain

$$\underset{x_k, k \in \mathcal{R}}{\text{minimize}} \quad \sum_{k \in \mathcal{R}} f_k(x_k) \tag{17a}$$

$$\text{subject to} \quad h_k(x_k) \leq 0, \quad \forall k \in \mathcal{R}, \tag{17b}$$

$$\sum_{k \in \mathcal{R}} A_k x_k = 0, \tag{17c}$$

which is an equivalent OPF formulation to (10), but in separable form.

IV. Distributed Optimization Algorithms

The general idea in solving (17) is to solve augmented regional OPFs and to penalize the deviation of (boundary) variables from a fixed auxiliary variable z, which is an information

stemming from neighboring regions. Note that we use

$$x = [x_1^\top \ ... \ x_R^\top]^\top \tag{18a}$$

$$z = [z_1^\top \ ... \ z_R^\top]^\top \tag{18b}$$

$$A = [A_1 \ ... \ A_R]. \tag{18c}$$

The regions then exchange information and, depending on the algorithm, z is updated in a specific way. The update is redistributed to the local agents for a new OPF calculation until consensus between regions is achieved. An overview on the implemented ADMM is given in Algorithm 1. As stated before, the main difference from ALADIN (see Algorithm 2) is the update of z. While (20) is a simple averaging step and entirely distributable [18], the quadratic problem (25) is a centralized step which relies on gradients (24b) and Hessians (24c) of the local problems. Note that the Hessians are required to be positive definite to ensure convergence [21]. Where necessary, we enforce this with a modified $LDL^\top$ Cholesky factorization [25]. An active set is formed in (25c), which ensures that e.g. linearized node balance equations are still fulfilled with an updated z. Furthermore, λ can trivially be computed in ADMM by (21), whereas in ALADIN it is a dual variable of the QP. In both algorithms, the penalty parameter ρ must be chosen carefully since it is widely known to be crucial for good convergence behavior [26]. In ALADIN, a weighting matrix Σ_k is introduced for each region k to numerically cope with different value ranges or importance for convergence. It is a diagonal matrix with varying entries depending on the related consensus variable. We adopt this approach to ADMM as well to scale the consensus constraints, only here we define one entry per constraint instead of per variable, which subsequently reduces the dimension of Σ_k. This novel scaling speeds up convergence considerably when using voltages *and* power injections as boundary variables. Matrix entries related to power are denoted with $\Sigma_k(S)$, and entries related to voltage are denoted with $\Sigma_k(V)$. In ADMM, an update rule on ρ can be useful to enforce consensus. In ALADIN, large values of μ may lead to numerical instability in the beginning of the algorithm. Therefore, as proposed in [23], we ramp up the parameter to the desired value during the first iterations. Deeper insights on similarities and differences between ALADIN and ADMM are found in [21].

Algorithm 1: ADMM.

1: **Initialization:** Initial guesses z_k, λ_k; penalty parameters $\rho_k = \rho$, local residues $\Gamma_k = \infty$, weighting matrices Σ_k, tolerance ϵ

2: **while** $||Ax||_\infty > \epsilon$ **do**

3: Solve for all $k \in \mathcal{R}$ the decoupled NLPs

$$\min_{x_k} f_k(x_k) + \lambda_k^\top A_k x_k + \frac{\rho_k}{2}||A_k(x_k - z_k)||^2_{\Sigma_k} \tag{19a}$$

$$\text{s.t. } h_k(x_k) \leq 0 \quad | \ \kappa_k \tag{19b}$$

4: Solve the coupled averaging step

$$\min_{z_k, k\in\mathcal{R}} \sum_{k\in\mathcal{R}} ||A_k(x_k - z_k)||_2^2 \tag{20a}$$

$$\text{s.t. } \sum_{k\in\mathcal{R}} A_k z_k = 0 \tag{20b}$$

5: Calculate for all $k \in \mathcal{R}$ dual variables

$$\lambda_k^+ = \lambda_k + \rho_k \Sigma_k A_k (x_k - z_k) \tag{21}$$

6: Calculate for all $k \in \mathcal{R}$ local residues and penalty parameter updates

$$\Gamma_k^+ = ||A_k(x_k - z_k)||_\infty \tag{22a}$$

$$\rho_k^+ = \begin{cases} ||\rho_k||_\infty & \text{if } \Gamma_k^+ \leq \Theta\Gamma_k \\ \tau||\rho_k||_\infty & \text{otherwise} \end{cases} \tag{22b}$$

7: Update for all $k \in \mathcal{R}$: $\lambda_k \leftarrow \lambda_k^+$, $\Gamma_k \leftarrow \Gamma_k^+$, $\rho_k \leftarrow \rho_k^+$

8: **end while**

V. Simulation Results

In the following, we will first present an illustrative 5-bus and a more realistic 66-bus test system. Then we will justify the use of scaled ADMM by means of an AC OPF comparison to unscaled ADMM. Finally, we will show detailed simulation results for both test systems under different partitioning approaches with scaled ADMM and ALADIN. The framework is modeled in MATLAB, and problems (10) (to obtain optimal solution x^*), (19) and (23) are solved with IPOPT [27]. Algorithm parameter settings are shown in Table II and we use the same cost coefficient for all reactive power injections ($a_\mathrm{Q} = 0.001\left[\frac{1}{\mathrm{Mvar}^2}\frac{\$}{\mathrm{h}}\right]$). The base power for p.u.-values is 100 MVA. Similarly to [23], we use the following quantities in order to depict convergence behavior:

- The deviation of optimization variables from the optimal value $||x - x^*||_\infty$.
- The fulfillment of consensus constraints $||Ax||_\infty$.
- The algorithm step size for the z-update $||d||_\infty$, with $d = A(x - z)$ (ADMM) or $d = x - z$ (ALADIN). Note that in ADMM, due to the averaging properties, $||d||_\infty = \frac{1}{2}||Ax||_\infty$.
- The first-order optimality condition violation $r = \max(||L_k||_\infty, k \in \mathcal{R})$ with $L_k = \nabla f_k(x_k) + \lambda_k^\top A_k x_k + \nabla h_k(x_k)\kappa_k$.
- The cost suboptimality $\tilde{f} = |1 - f/f^*|$.

A. Test Systems

1) 5-Bus: The AC system is based on [28], which was also used in [22], [23]. It is divided into three control areas and has a total system load of 1000 MW. It consists of a generation center and load center, which makes it challenging for distributed power flow approaches. We assume the same quadratic generator cost functions as in [22] (see Table III). Next, we extend the network by connecting a 3-bus 300 kV DC grid via three converters, a schematic topology overview is shown in Fig. 5. We assume a DC line resistance of $R = 0.002$ p.u. and a nominal converter rating of $\overline{S}_\mathrm{VSC} = 100$ MVA. The converter loss

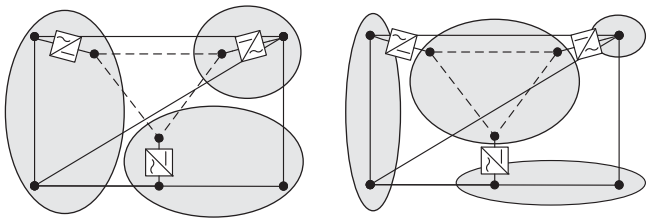

Fig. 5. Schematic topology of 5-bus AC test system [28] with connected 3-bus DC system (dashed lines). Circles depict the region partitioning according to the chosen decoupling approach. Left: *Shared-DC*, right: *Joint-DC*.

Algorithm 2: ALADIN.

1: **Initialization:** Initial guesses z_k, λ_k; penalty parameters ρ, $\mu = \underline{\mu}$; weighting matrices Σ_k; tolerance ϵ

2: **while** $||Ax||_\infty > \epsilon$ and $||x - z||_\infty > \epsilon$ **do**

3: Solve for all $k \in \mathcal{R}$ the decoupled NLPs

$$\min_{x_k} f_k(x_k) + \lambda^\top A_k x_k + \frac{\rho}{2}||x_k - z_k||^2_{\Sigma_k} \tag{23a}$$

$$\text{s.t. } h_k(x_k) \leq 0 \quad | \kappa_k \tag{23b}$$

4: Compute for all $k \in \mathcal{R}$ Jacobians, gradients and Hessians

$$C_{k,j} = \begin{cases} \frac{\partial}{\partial y}(h_k(y))_j|_{y=x_k} & \text{if } (h_k(x_k))_j = 0 \\ 0 & \text{otherwise} \end{cases} \tag{24a}$$

$$g_k = \nabla f_k(x_k) \tag{24b}$$

$$H_k = \nabla^2\{f_k(x_k) + \kappa_k^\top h_k(x_k)\} \tag{24c}$$

5: Solve coupled quadratic problem

$$\min_{\Delta x, s} \sum_{k\in\mathcal{R}} \left\{ \frac{1}{2}\Delta x_k^\top H_k \Delta x_k + g_k^\top \Delta x_k \right\} + \lambda^\top s + \frac{\mu}{2}||s||_2^2 \tag{25a}$$

$$\text{s.t. } \sum_{k\in\mathcal{R}} A_k(x_k + \Delta x_k) = s \quad | \lambda_{\text{QP}} \tag{25b}$$

$$C_k \Delta x_k = 0, \quad k \in \mathcal{R} \tag{25c}$$

6: Update $z \leftarrow x + \Delta x$, $\lambda \leftarrow \lambda_{\text{QP}}$, $\mu \leftarrow \min(\overline{\mu}, r_\mu \mu)$

7: **end while**

function is based on [29] and defined as

$$P_{\text{VSCL}} = \left(0.01103 + 0.0075\left(\frac{|S_{\text{VSC}}|}{\overline{S}_{\text{VSC}}}\right)^2\right)\overline{S}_{\text{VSC}}, \tag{26}$$

which leads to 1.103% of constant losses and an efficiency of 98.15% at full load. Voltage limits are 0.9 to 1.1 p.u. on the AC side and 0.95 to 1.05 p.u. on the DC side. The centralized solution gives a total generated power of 1009.81 MW at costs of 21373.41 \$/h.

2) 66-Bus Test System: In [30], a hybrid AC-DC benchmark system consisting of three control areas is presented. There is a desired power imbalance between the individual areas to force a significant long-distance power transfer, which makes the system interesting for distributed algorithm studies. We amplify this effect by adding higher generator costs in the load center (see Table III). Generally, the coefficients are in the range of the 5-bus system with a small random deviation. We choose *Stage 2* of three available DC systems, which is a grid extension to include all VSCs in one system. Furthermore, we neglect bus 67, which is a supplementary offshore wind park and the rated converter power is set to $\overline{S}_{\text{VSC}} = 1800$ MVA for all VSCs. Lastly, while in [30] converter losses are neglected, we use loss function (26). The centralized solution gives a total generated power of 9530.06 MW at costs of 209169.32 \$/h.

B. Scaled vs. Unscaled ADMM

First, we will show a short comparison between scaled and unscaled ADMM. To foster a fair comparison, we tuned parameters (see Table II) for both algorithms and allowed for penalty updates with traditional unscaled ADMM, which are not necessary with scaled ADMM in this work. Performance indices for both test systems (without HVDC extension) are shown in Fig. 6. With scaled ADMM, it can be observed how fewer iterations are necessary until consensus ($||Ax||_\infty$) is satisfactory to allow for a feasible power flow. Also, the distance from solution x to the centrally computed minimizer x^* is smaller. Nevertheless, the optimality gap is acceptable with both versions. This general convergence behavior was observed in a broader range of test cases but would go beyond the scope of this work and we will continue with the scaled ADMM version.

C. Scaled ADMM vs. ALADIN

1) 5-Bus System: In Fig. 7, variable convergence behavior is shown for the *Joint-DC* approach. All variables eventually converge to its (centrally computed) optimal value for both ADMM and ALADIN. In ADMM, generator power, which has the largest impact on objective function, reaches near-optimality after 20 iterations. The remaining variables, i.e. converter power and voltages, require many more iterations. In ALADIN, all variables reach near-optimality after 6-7 iterations.

When we use the *Shared-DC* approach, the results are generally similar, see Fig. 8. However, due to the different decomposition approach, the progression differs for variables directly related to the DC side, i.e. $P_{\text{VSC}}, Q_{\text{VSC}}$ and V_{DC}.

The general convergence behavior for the quantities stated at the beginning of the chapter is shown in Fig. 9. For comparison, we add the results for the original AC test system without DC grid (*"AC"*). It is notable that in both ADMM and ALADIN, convergence properties are similar among the three decomposition approaches. The difference between ADMM and ALADIN however, is significant. The consensus error falls below the criteria of $\epsilon = 10^{-4}$ after 10–11 iterations in ALADIN and after 185-189 iterations in ADMM, while the objective suboptimality is in the range of 10^{-5}% for ALADIN and 10^{-3}% for ADMM. Also, first-order optimality condition violation and the variable suboptimality are considerably smaller in ALADIN. Solely the algorithm step size $||d||_\infty$ reaches the same range.

2) 66-Bus System: Convergence behavior is shown in Fig. 10. Iteration numbers differ between 106 and 142 iterations with ADMM, and ALADIN struggles slightly longer with the *AC* case compared to both *DC* cases. Nevertheless, the centrally

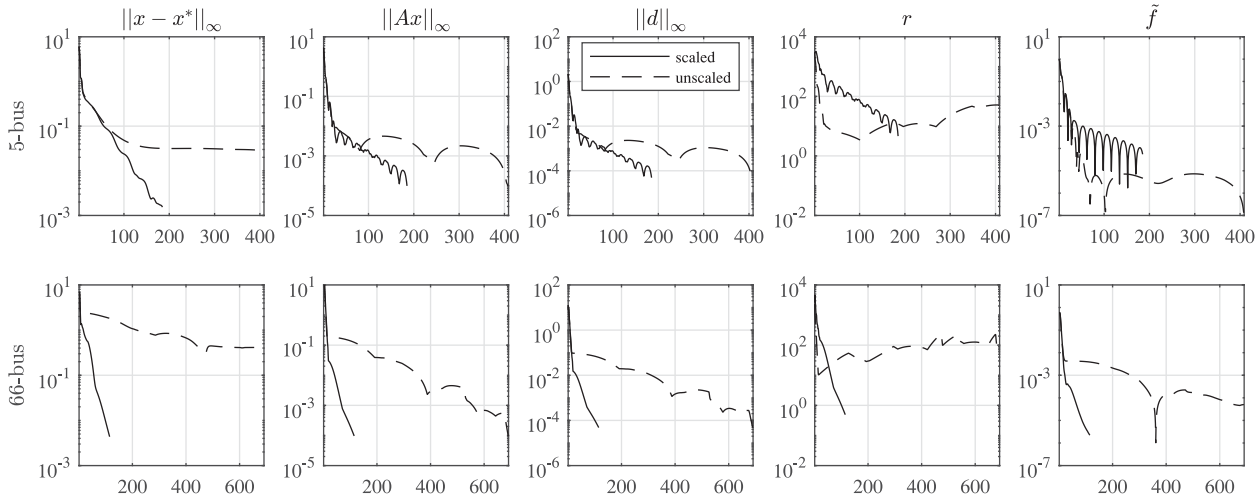

Fig. 6. Convergence behavior of unscaled ADMM (dashed) and scaled ADMM (solid).

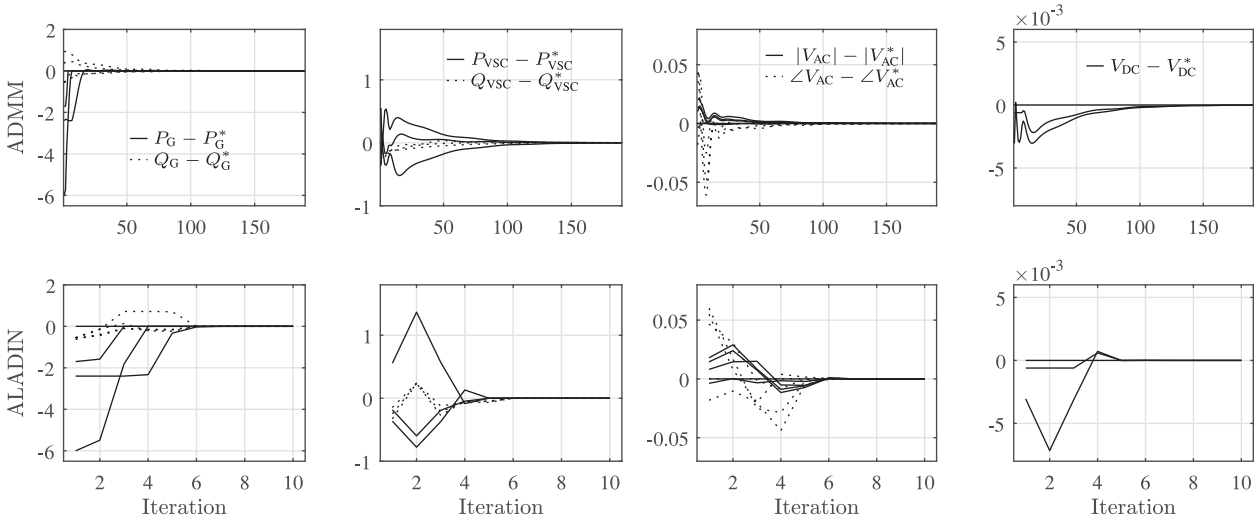

Fig. 7. Variable convergence towards optimal value of ADMM (top) and ALADIN (bottom) for the 5-bus system with *Joint-DC* approach.

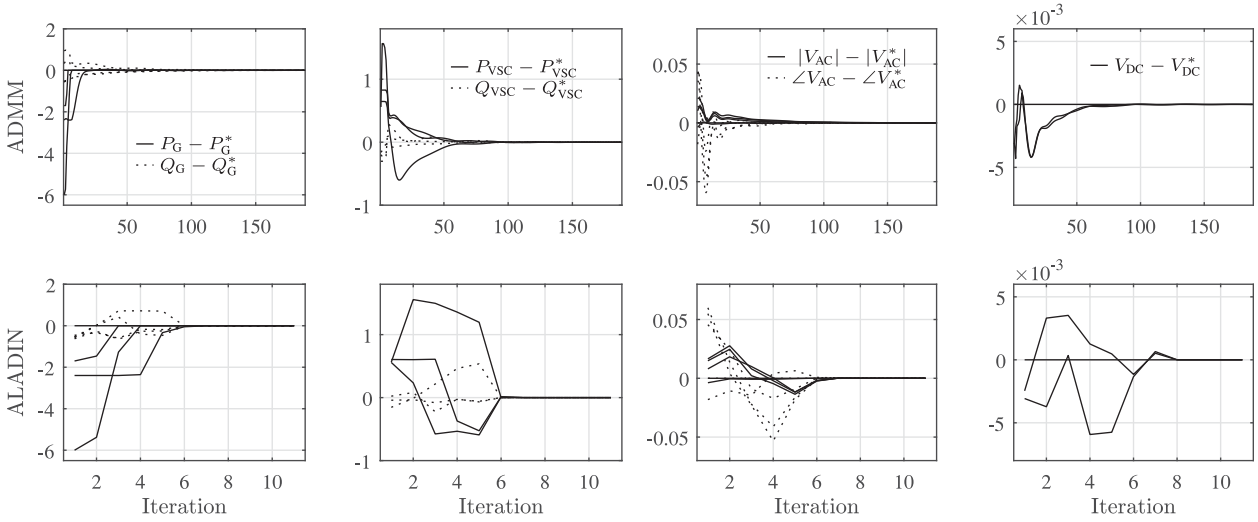

Fig. 8. Variable convergence towards optimal value of ADMM (top) and ALADIN (bottom) for the 5-bus system with *Shared-DC* approach.

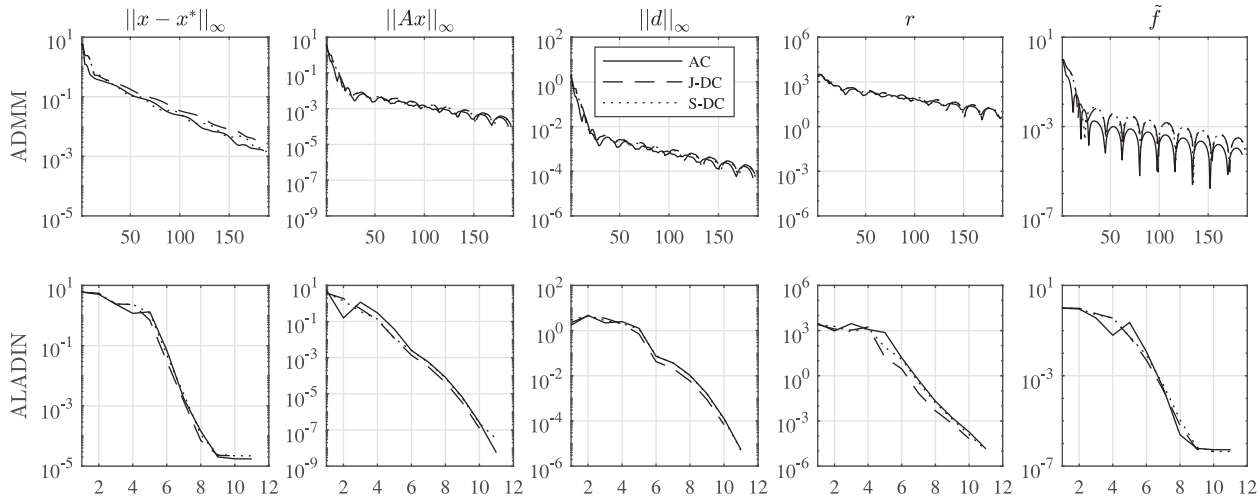

Fig. 9. Convergence behavior of ADMM (top) and ALADIN (bottom) for the 5-bus system. Solid: *AC*, dashed: *Joint-DC*, dotted: *Shared-DC*.

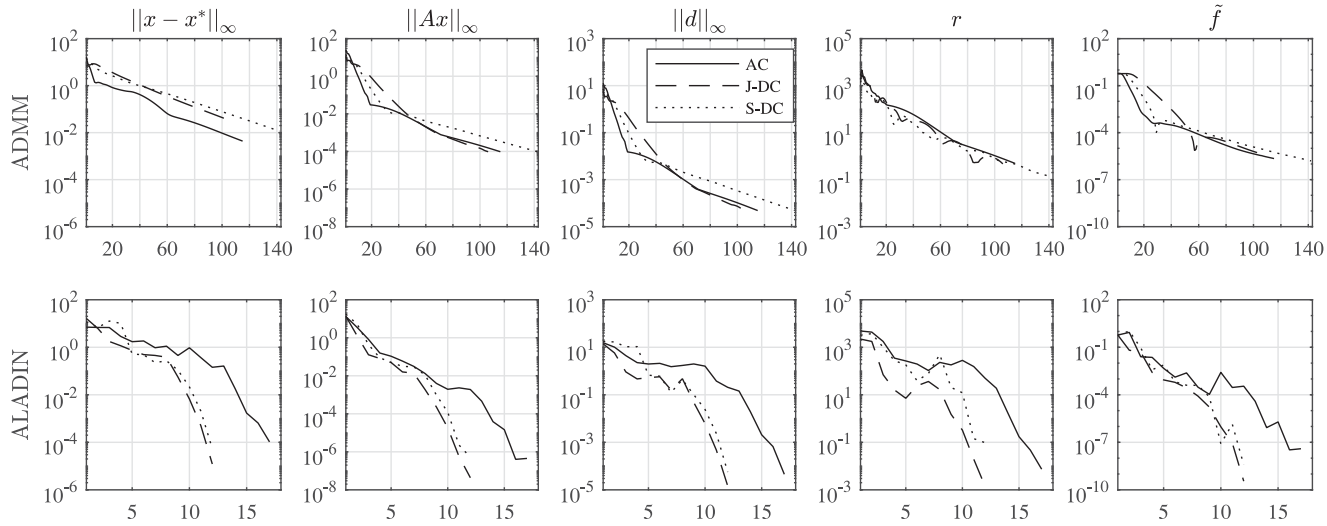

Fig. 10. Convergence behavior of ADMM (top) and ALADIN (bottom) for the 66-bus system. Solid: *AC*, dashed: *Joint-DC*, dotted: *Shared-DC*.

TABLE I
ITERATION NUMBERS, WALL CLOCK TIME t AND COST SUBOPTIMALITY UNDER VARIED TEST SYSTEMS AND PARTITIONING APPROACHES

Case		ADMM			ALADIN		
		# it.	t [s]	$\tilde{f}$	# it.	t [s]	$\tilde{f}$
5-b.	*AC*	185	17.7	5.5e−5	11	1.2	5.3e−7
	J-DC	189	25.6	5.5e−5	10	1.6	4.5e−7
	S-DC	188	21.3	8.5e−5	11	1.5	4.5e−7
66-b.	*AC*	115	14.6	2.2e−6	17	2.9	3.9e−8
	J-DC	106	14.7	4.3e−6	12	2.4	3.5e−10
	S-DC	142	21.4	1.6e−6	12	2.8	3.8e−9

computed objective value is again reached with high accuracy for all ADMM and ALADIN cases (deviation below $10^{-3}\%$ and $10^{-5}\%$, respectively).

3) Summary: Results for both systems are summarized in Table I. It is notable that even though ten times larger in terms of buses and system load, fewer ADMM iterations are required in the 66-bus case compared to the 5-bus case. ALADIN iterations are in the same range, except for the *AC* case. Since only 5 out of 66 AC buses are boundary buses compared to 4 out of 5 AC buses in the smaller case, one could presume the larger case to be more weakly coupled and thus less challenging for distributed optimization. Wall clock times are given for calculations on an Intel(R) Core(TM) i7-3630QM CPU at 2.40 GHz with 16 GB RAM. The computational costs per iteration are only slightly higher for ALADIN in our test systems, which leads to a strong wall clock time decrease. A total speedup factor between 14–16 is achieved for the 5-bus cases and a factor between 5–8 is achieved for the 66-bus cases.

VI. DISCUSSION & OUTLOOK

This paper addresses the field of distributed optimal power flow in hybrid AC-DC grids, which is based on a full AC OPF throughout the work. However, policies might implicate limited control over generating units. Thus, our method could also be

TABLE II
PARAMETER SETTINGS FOR ADMM AND ALADIN

Parameter	unscaled ADMM		scaled ADMM		ALADIN	
	5-bus	66-bus	5-bus	66-bus	5-bus	66-bus
ρ	10^4	10^3	10^3	10^2	10^3	10^2
$\Sigma_k(S)$	1	1	1	1	1	1
$\Sigma_k(V)$	1	1	10^2	10^2	10^2	10^2
τ	1.02	1.02	1	1	-	-
Θ	0.99	0.99	1	1	-	-
$\underline{\mu}$	-	-	-	-	10^3	10^3
$\overline{\mu}$	-	-	-	-	10^6	10^6
r_μ	-	-	-	-	2	2

TABLE III
GENERATOR COST COEFFICIENTS

Generator		cost coefficient	
		$a_{\mathrm{G}}\left[\frac{1}{\mathrm{MW}^2}\frac{\$}{\mathrm{h}}\right]$	$b_{\mathrm{G}}\left[\frac{1}{\mathrm{MW}}\frac{\$}{\mathrm{h}}\right]$
5-bus	1	0.010	15
	2	0.011	30
	3	0.012	40
	4	0.013	10
66-bus	1	0.0141	14.1
	2	0.0145	14.5
	3	0.0106	10.6
	4	0.0146	14.6
	5	0.0132	13.2
	6	0.0105	10.5
	7	0.0164	16.4
	8	0.0177	17.7
	9	0.0198	19.8
	10	0.0198	19.8
	11	0.0158	15.8
	12	0.0199	19.9
	13	0.0148	14.8
	14	0.0124	12.4
	15	0.0140	14.0
	16	0.0107	10.7
	17	0.0121	12.1

applied when TSOs seek to optimize AC-DC converter set points in a distributed manner, without changing the power output of (most of the) power plants.

We tested our methods on two different systems, but additional case studies are necessary to further investigate convergence properties and dependencies on parameter settings. This includes varying the cost coefficients and increasing the grid size, since realistic transmission systems have hundreds or thousands of buses. With increasing system sizes, the computational costs for the central step are expected to grow faster for ALADIN relative to ADMM. Thus, the interplay of iteration numbers and computational costs per iteration in large-scale systems will be of interest for future studies.

Line flow limits will be implemented as a next step, and the model can be further extended by n-1-security constraints to cover important security-related concerns of the TSOs.

While ADMM is fully distributable, i.e. there is no central entity mandatory for coordination, ALADIN still relies on a centralized update step. Also, each TSO must provide sensitive information such as generator cost functions or shadow prices of each node, which could be a privacy concern. These issues require further investigations on how to minimize necessary information exchange.

REFERENCES

[1] J. Carpentier, "Contribution a l'etude du dispatching economique," *Bull. de la Societe Francaise des. Electriciens*, vol. 3, pp. 431–447, Aug. 1962.

[2] J. Momoh, R. Adapa, and M. El-Hawary, "A review of selected optimal power flow literature to 1993. I. Nonlinear and quadratic programming approaches," *IEEE Trans. Power Syst.*, vol. 14, no. 1, pp. 96–104, Feb. 1999.

[3] J. Momoh, M. El-Hawary, and R. Adapa, "A review of selected optimal power flow literature to 1993. II. Newton, linear programming and interior point methods," *IEEE Trans. Power Syst.*, vol. 14, no. 1, pp. 105–111, Feb. 1999.

[4] R. Wiget and G. Andersson, "Optimal power flow for combined ac and multi-terminal HVDC grids based on VSC converters," in *Proc. IEEE Power Energy Soc. General Meeting*, Jul. 2012, pp. 1–8.

[5] M. Baradar, M. R. Hesamzadeh, and M. Ghandhari, "Second-order cone programming for optimal power flow in VSC-type ac–dc grids," *IEEE Trans. Power Syst.*, vol. 28, no. 4, pp. 4282–4291, Nov. 2013.

[6] J. Cao, W. Du, H. F. Wang, and S. Q. Bu, "Minimization of transmission loss in meshed ac/dc grids with VSC-MTDC networks," *IEEE Trans. Power Syst.*, vol. 28, no. 3, pp. 3047–3055, Aug. 2013.

[7] A. K. Marten and D. Westermann, "Schedule for converters of a meshed HVDC grid and a contingency schedule for adaption to unscheduled power flow changes," in *Proc. IEEE Power Energy Soc. General Meeting*, Jul. 2013, pp. 1–5.

[8] W. Feng, L. A. Tuan, L. B. Tjernberg, A. Mannikoff, and A. Bergman, "A new approach for benefit evaluation of multiterminal VSC-HVDC using a proposed mixed ac/dc optimal power flow," *IEEE Trans. Power Del.*, vol. 29, no. 1, pp. 432–443, Feb. 2014.

[9] N. Meyer-Huebner, F. Gielnik, M. Suriyah, and T. Leibfried, "Dynamic optimal power flow in ac networks with multi-terminal HVDC and energy storage," in *Proc. IEEE Innovative Smart Grid Technologies—Asia*, Nov. 2016, pp. 300–305.

[10] N. Meyer-Huebner *et al.*, "N-1-secure dispatch strategies of embedded HVDC using optimal power flow," in *Proc. IEEE Power Energy Soc. General Meeting*, 2018, pp. 1–5.

[11] B. H. Kim and R. Baldick, "A comparison of distributed optimal power flow algorithms," *IEEE Trans. Power Syst.*, vol. 15, no. 2, pp. 599–604, May 2000.

[12] D. K. Molzahn *et al.*, "A survey of distributed optimization and control algorithms for electric power systems," *IEEE Trans. Smart Grid*, vol. 8, no. 6, pp. 2941–2962, Nov. 2017.

[13] A. J. Conejo, F. J. Nogales, and F. J. Prieto, "A decomposition procedure based on approximate Newton directions," *Math. Program.*, vol. 93, no. 3, pp. 495–515, Dec. 2002. [Online]. Available: https://doi.org/10.1007/s10107-002-0304-3

[14] G. Hug-Glanzmann and G. Andersson, "Decentralized optimal power flow control for overlapping areas in power systems," *IEEE Trans. Power Syst.*, vol. 24, no. 1, pp. 327–336, Feb. 2009.

[15] F. J. Nogales, F. J. Prieto, and A. J. Conejo, "A decomposition methodology applied to the multi-area optimal power flow problem," *Ann. Operations Res.*, vol. 120, no. 1, pp. 99–116, Apr. 2003. [Online]. Available: https://doi.org/10.1023/A:1023374312364

[16] B. H. Kim and R. Baldick, "Coarse-grained distributed optimal power flow," *IEEE Trans. Power Syst.*, vol. 12, no. 2, pp. 932–939, May 1997.

[17] R. Baldick, B. H. Kim, C. Chase, and Y. Luo, "A fast distributed implementation of optimal power flow," *IEEE Trans. Power Syst.*, vol. 14, no. 3, pp. 858–864, Aug. 1999.

[18] T. Erseghe, "Distributed optimal power flow using ADMM," *IEEE Trans. Power Syst.*, vol. 29, no. 5, pp. 2370–2380, Sep. 2014.

[19] T. Erseghe, "A distributed approach to the OPF problem," *EURASIP J. Advances Signal Process.*, vol. 2015, no. 1, May 2015, Art. no. 45.

[20] J. Guo, G. Hug, and O. K. Tonguz, "A case for nonconvex distributed optimization in large-scale power systems," *IEEE Trans. Power Syst.*, vol. 32, no. 5, pp. 3842–3851, Sep. 2017.

[21] B. Houska, J. Frasch, and M. Diehl, "An augmented Lagrangian based algorithm for distributed nonconvex optimization," *SIAM J. Optim.*, vol. 26, pp. 1101–1127, Apr. 2016.

[22] A. Engelmann, T. Mühlpfordt, Y. Jiang, B. Houska, and T. Faulwasser, "Distributed ac optimal power flow using ALADIN," *IFAC-PapersOnLine*, vol. 50, pp. 5536–5541, Jul. 2017.

[23] A. Engelmann, Y. Jiang, T. Mühlpfordt, B. Houska, and T. Faulwasser, "Toward distributed OPF using ALADIN," *IEEE Trans. Power Syst.*, vol. 34, no. 1, pp. 584–594, Jan. 2019.

[24] E. Iggland, R. Wiget, S. Chatzivasileiadis, and G. Anderson, "Multi-area DC-OPF for HVAC and HVDC grids," *IEEE Trans. Power Syst.*, vol. 30, no. 5, pp. 2450–2459, Sep. 2015.
[25] P. Gill, W. Murray, and M. Wright, *Practical Optimization*. London, U.K.: Academic, 1981.
[26] S. Mhanna, A. C. Chapman, and G. Verbič, "A component-based dual decomposition method for the OPF problem," *Sustain. Energy, Grids, Netw.*, vol. 16, pp. 91–110, 2018, doi: 10.1016/j.segan.2018.04.003.
[27] A. Wächter and L. T. Biegler, "On the implementation of an interior-point filter line-search algorithm for large-scale nonlinear programming," *Math. Program.*, vol. 106, no. 1, pp. 25–57, Mar. 2006. doi: 10.1007/s10107-004-0559-y.
[28] F. Li and R. Bo, "Small test systems for power system economic studies," in *Proc. IEEE Power Energy Soc. General Meeting*, Jul. 2010, pp. 1–4.
[29] G. Daelemans, K. Srivastava, M. Reza, S. Cole, and R. Belmans, "Minimization of steady-state losses in meshed networks using VSC HVDC," in *Proc. IEEE Power Energy Soc. General Meeting*, Jul. 2009, pp. 1–5.
[30] F. Sass, T. Sennewald, A. K. Marten, and D. Westermann, "Mixed ac high-voltage direct current benchmark test system for security constrained Optimal Power Flow calculation," *IET Gener., Transmiss. Distribution*, vol. 11, no. 2, pp. 447–455, 2017.

Nico Meyer-Huebner was born in Bad Hersfeld, Germany, in 1986. He received the Dipl.Ing. degree in electrical engineering from the Karlsruhe Institute of Technology, Karlsruhe, Germany, in 2013, where he is currently working toward the Ph.D. degree in electrical engineering. His research interests include power system analysis, optimal operation of future transmission systems, and distributed optimization. He is a member of VDE.

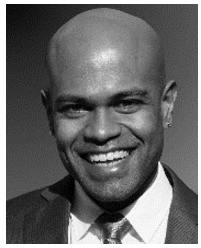

Michael Suriyah (M'14) was born in Kuala Lumpur, Malaysia, in 1982. He received the Diploma and M.Sc. degrees in electrical engineering from the University of Applied Sciences, Karlsruhe, Germany, in 2007 and 2008, respectively, and the Ph.D. degree in electrical engineering from the Karlsruhe Institute of Technology, Karlsruhe, Germany, in 2013. Currently, he is the Head of the Department for Power Networks, Institute of Electric Energy Systems and High-Voltage Technology, Karlsruhe Institute of Technology. His research interests include aging diagnostics and onsite testing of power transformers, high-voltage testing methods, analysis of electric power networks as well as planning of future power systems. He is a member of VDE.

Thomas Leibfried (M'96) was born in Neckarsulm, Germany, in 1964. He received the Dipl.Ing. and Dr. Ing. degrees from the University of Stuttgart, Stuttgart, Germany, in 1990 and 1996, respectively. From 1996 to 2002, he was with Siemens AG, Nuremberg, Germany, working in the power transformer business in various technical and management positions. In 2002, he joined the University of Karlsruhe, Karlsruhe, Germany, as the Head of the Institute of Electric Energy Systems and High-Voltage Technology. He is a member of VDE and CIGRE.